CrystEngComm

Accepted Manuscript

ROYAL SOCIETY OF CHEMISTRY

www.rsc.org/crystengcomm

CrystEngComm

RSCPublishing

ARTICLE

Synthesis, crystal growth, and second-order nonlinear optical properties of new configurationally locked polyene derivatives†

Cite this: DOI: 10.1039/x0xx00000x

Xinyuan Zhang,[a, b] Xingxing Jiang, [a, b] Yin Li, *[a] Zheshuai Lin,[a] Guochun Zhang, [a] and Yicheng Wu[a]

Received 00th January 2012,
Accepted 00th January 2012

DOI: 10.1039/x0xx00000x

www.rsc.org/

Five new crystals based on configurationally locked polyene (CLP) chromophores structure are synthesized. This series of chromophores crystals all consists of a π-conjugated hexatriene bridge between the dicyanomethylidene electron acceptor and the electron donors with strong hyperpolarization. In particular, the acentric 2-(3-(4-phenylstyryl)-5, 5-dimethylcyclohex-2-enylidene) malononitrile (PSDCM) exhibits a large powder second-harmonic generation intensity about 0.3 × OH1 (a commonly used CLP nonlinear optical crystal), and the mechanism is elucidated by the first-principles studies. The single crystal X-ray diffraction, diffuse reflectance spectroscopy and thermal properties in PSDCM are characterized.

Introduction

Organic nonlinear optical (NLO) crystals have attracted much attention because of their potentials for various optical applications, such as photonic devices, optical parametric oscillation, frequency conversion, and THz wave generation and detection. [1-3] Compared to inorganic counterparts, organic NLO materials are of extensive interest due to their almost unlimited design possibility, easy synthesis, large nonlinear optical susceptibility and ultrafast response time. [4, 5] Recently, quite a few organic crystals exhibiting large macroscopic optical nonlinearities have been developed. For instance, the ionic stilbazolium salts crystal N, N-dimethylamino-N'-methylstilbazolium 4-methylbenzenesulfonate (DAST), N, N-dimethylamino-N'-methylstilbazolium 2, 4, 6-trimethylbenzenesulfonate (DSTMS), and the configurationally locked polyene (CLP) crystal 2-(3-(4-hydroxystyryl)-5, 5-dimethylcyclohex-2-enylidene) malononitrile (OH1) have very large NLO susceptibilities ($\chi^{(2)}_{ijk}$ > 240 pm/V at 1.9 μm) and large electro-optic coefficients (r_{ijk} > 50 pm/V at 1.3 μm), so they are very suitable for THz generation by optical rectification and difference frequency generation. [6-15]

It is well known that the CLP crystals are very promising for achieving highly polar chromophores molecules and forming acentric structure, which is greatly beneficial to the generation of large optical nonlinearities. The extensive investigations in this system have resulted in the development of some organic crystals with good NLO performance, e.g., verbenone-based DAV1, and other methylcyclohexenone-based OH2, MH2, OH3, PyM3, besides the isophorone-based OH1, PyT1, PyT3, MOT1, and DAT2. [16-22] In these CLP crystals, the electron donors are typically hydroxyl groups and the electron acceptor is a dicyanomethylidene [>C═C(CN)$_2$] group, which are connected by a π-conjugated hexatriene bridge.

Herein we report the discovery of six new isophorone-based CLP compounds with different electron donor groups, varied from phenyl, mercapto, tert-butyl, thienyl, to methyl-thienyl. In particular, one phase of the 2-(3-(4-phenylstyryl)-5, 5-dimethylcyclohex-2-enylidene) malononitrile (PSDCM) crystal exhibits a large powder second harmonic generation (SHG) intensity. Its diffuse reflectance spectroscopy and thermal properties have been measured and compared with those in OH1. Moreover, its NLO mechanism has been investigated by the first-principles studies.

Experimental Section

Synthesis and crystal growth

All reagents were purchased as high purity from Alfa Aesar, TCI Shanghai, and Sinopharm Chemical Reagent, and used without further purification. The synthetic route of PSDCM is shown in Fig. 1 as an example. All the compounds were synthesized by Knoevenagel condensations from the corresponding aldehyde and the intermediate 2-(3,5,5-trimethylcyclohex-2-enylidene) malononitrile. [23] The products were purified several times by recrystallization in methanol or dichloromethane. By changing the electron donor groups from phenyl, mercapto, tert-butyl, thienyl, to methyl-thienyl, five

new organic compounds have been synthesized. They are PSDCM (Phases I and II), 2-(5,5-dimethyl-3- (4-(methylthio)styryl)cyclohex-2-enylidene) malononitrile (DMSCM), 2-(3-(4-(tert- butyl)styryl)-5,5-dimethylcyclohex-2-enylidene) malononitrile (TSDCM), 2-(5,5- dimethyl-3-(2-(thiophen-2-yl)vinyl)cyclohex-2-enylidene) malononitrile (DTCM), and 2-(5,5-dimethyl-3-(2-(5-methylthiophen-2-yl)vinyl)cyclohex-2-enylidene) malononitrile (MTDCM). In order to confirm the successful synthesis of the target compounds, ^{1}H-nuclear magnetic resonance (NMR) spectra were recorded on Bruker Avance 400 Spectrometer on $CDCl_3$ solution.

PSDCM ^{1}H NMR (400 MHz, $CDCl_3$) δ 7.67 – 7.57 (m, 6H, Ar-H), 7.47 (t, J = 7.5 Hz, 2H, Ar-H), 7.38 (t, J = 7.3 Hz, 1H, Ar-H), 7.07 (q, J = 16.1 Hz, 2H, -CH=CH-), 6.87 (s, 1H, -C=CH-), 2.62 (s, 2H, $-CH_2$), 2.50 (s, 2H, $-CH_2$), 1.10 (s, 6H, $-CH_3$).

DMSCM ^{1}H NMR (400 MHz, $CDCl_3$) δ 7.42 (d, *J* = 8.5 Hz, 2H, Ar-H), 7.24 (d, *J* = 8.5 Hz, 2H, Ar-H), 6.98 (q, *J* = 16.1 Hz, 2H, -CH=CH-), 6.83 (s, 1H, -C=CH-), 2.60 (s, 2H, $-CH_2$), 2.52 (s, 3H, $-CH_3$), 2.46 (s, 2H, $-CH_2$), 1.08 (s, 6H, $-CH_3$).

TSDCM ^{1}H NMR (400 MHz, $CDCl_3$) δ 7.42 (t, J = 7.8 Hz, 4H, Ar-H), 7.07 – 6.93 (m, 2H, -CH=CH-), 6.83 (s, 1H, -C=CH-), 2.60 (s, 2H, $-CH_2$), 2.47 (s, 2H, $-CH_2$), 1.34 (s, 9H, $-C(CH_3)_3$), 1.08 (s, 6H, $-CH_3$).

DTCM ^{1}H NMR (400 MHz, $CDCl_3$) δ 7.37 (d, *J* = 5.0 Hz, 1H, -CH=CH-), 7.19 (dd, *J* = 9.7, 6.1 Hz, 2H, $-C_4H_3S$), 7.06 (dd, *J* = 5.0, 3.7 Hz, 1H, -CH=CH-), 6.81 (s, 1H, $-C_4H_2S$), 6.76 (s, 1H, -C=CH-), 2.59 (s, 2H, $-CH_2$), 2.42 (s, 2H, $-CH_2$), 1.07 (s, 6H, $-CH_3$).

MTDCM ^{1}H NMR (400 MHz, $CDCl_3$) δ 7.11 (d, J = 15.7 Hz, 1H, -CH=CH-), 6.99 (d, J = 3.6 Hz, 1H, $-C_4H_2S$), 6.77 (s, 1H, -C=CH-), 6.71 (dd, J = 3.6, 1.0 Hz, 1H, $-C_4H_2S$), 6.64 (d, J = 15.8 Hz, 1H, -CH=CH-), 2.58 (s, 2H, $-CH_2$), 2.52 (s, 3H, $-CH_3$), 2.40 (s, 2H, $-CH_2$), 1.06 (s, 6H, $-CH_3$).

The five new crystals could be obtained by slow evaporation method or cooling method. However, the morphologies of PSDCM crystals are influenced by different solvents. In dichloromethane solvent yellow plate single crystals of PSDCM (PSDCM-(I) phase) are obtained (Fig. 2 (a)), which are different from the strip crystals grown via cooling method from acetonitrile (PSDCM-(II) phase), as shown in Fig. 2 (b). Note that the different colors displayed in the photos are mainly due to the different angles of view of the cameras and the different thickness of the two crystals.

X-Ray structure determination

All X-ray data of the obtained crystals were collected with graphite-monochromatized Mo Kα (λ = 0.71073 Å) at 153 K on a Rigaku AFC10 diffractometer equipped with a Saturn CCD detector. The collection of the intensity data was carried out with the program Crystalclear. Cell refinement and data reduction were carried out with the use of the program Crystalclear. The structure was solved by direct methods. All of the hydrogen atoms were located on a difference Fourier. The crystallographic data for the five CLP crystals are listed in Table 1 and the relevant CIF files are given in the Supporting Information. It is clear that except the PSDCM-(I) phase the other five compounds are centrosymmetric and have no SHG effect.

Characterizations

A LabsysTM TG–DTA16 (SETARAM) thermal analyzer was used to investigate the thermal property by the differential scanning calorimetric (DSC) analysis at a heating rate of 10 °C min^{-1} in nitrogen. The thermal gravimetric analysis (TGA) was performed on a Perkin-Elmer Diamond TG/DTA spectrometer, and a heating rate of 10 °C min^{-1} in nitrogen was adopted. The DSC results of all the five crystals are listed in Table 2.

A Cary 1E UV−visible spectrophotometer with a diffuse reflectance accessory was used to measure the spectra of PSDCM-(I) and OH1 in the range of 300 nm (4.13 eV) - 1000 nm (1.24 eV). The maximum absorption wavelengths of the five crystals in methanol were also measured using Cary 1E UV−visible spectrophotometer.

Optical SHG tests of PSDCM were performed on the powder samples by means of the Kurtz-Perry method. [24] Fundamental 2.09 μm light was generated with a Q-switched Ho:Tm:Cr:YAG laser. The PSDCM-(I) crystalline powder was prepared by mechanical grinding of single crystals.

First-principles method

To explore the mechanism of the optical nonlinearity in the acentric PSDCM-(I) crystal, the first-principles calculations were performed using CASTEP, a plane-wave pseudopotential total energy package based on the density functional theory (DFT). [25,26] The local density approximation (LDA) functionals developed by Ceperley, Alder Perdew and Zunger (CA-PZ), was used to describe the exchange-correlation energy. [27] The ultrasoft pseudopotential was adopted to treat the interaction between the valence electrons (H 1s, C 2s2p, O 2s4p, and N 2s2p electrons) and atomic kernels. [28] To guarantee the computational accuracy, the kinetic energy cutoff 350eV and intensive Monkhorst-pack k-point meshes spanning less than 0.04 $Å^{-1}$ in the Brillouin zone were chosen. [29] It is well known that the band gaps predicted by LDA-DFT are smaller than the measured values, so the scissor operators (0.43eV and 0.37eV for PSDCM-(I) and OH1, respectively) were adopted to shift all the conduction bands to match the calculated band gaps with the experimental ones. Based on the scissor-corrected electronic structure, the static SHG coefficients were calculated by the formula from the Ref 30.

Results and Discussion

The chemical structures of PSDCM, DMSCM, TSDCM, DTCM, and MTDCM are shown in Fig. 3. The chromophore structure consists of the configurationally locked π-conjugated hexatriene bridge linked between dicyanomethylidene [>C=C$(CN)_2$] electron acceptor and electron donor, which are phenyl, mercapto, tert-butyl, thienyl, and methyl-thienyl, respectively. It is anticipated that all these molecules would possess large microscopic second first hyperpolarizability due

to the strong polarization of acceptor and donor functional groups. Unfortunately, these organic compounds are all crystallized in the centrosymmetric space groups except one phase in PSDCM. Thus, in the following section the structural, thermal and optical properties in the PSDCM crystals are mainly concerned.

PSDCM has two different crystal forms: PSDCM-(I) crystal obtained by slow evaporation belongs to noncentrosymmetric structures with space group $P2_1$, while PSDCM-(II) crystal grown from acetonitrile solvent possess centrosymmetric space group $P2_1/c$. A single molecular conformation and atom-numbering scheme for PSDCM in the crystalline state is shown in Fig. 4. Actually, the molecular conformation in PSDCM-(I) phase is slightly different from that in PSDCM-(II) phase. In both phases, the phenyl ring (C7-C12) and donor phenyl group (C1-C6) are almost planar, but in PSDCM-(I) phase the angle between two phenyl planes is 4.6°, while in PSDCM-(II) phase the angle is 3.9°. Meanwhile, in PSDCM-(I) phase the double bonds in the hexene ring and dicyanomethylidene acceptor are also nearly planar, but lie slightly out of the phenyl plane (C7-C12) at an angle of 9.7°, while in PSDCM-(II) phase the angle is 10.2°.

In both PSDCM phases, every two PSDCM molecules form acentric molecular pairs stacked up one by one (see Fig. 5). In each pair of the PSDCM molecules, two PSDCM molecules link head to tail, while the two molecule planes are in the angle of 65°. The main molecular interaction in PSDCM pairs is resulted from the weak head-to-tail hydrogen bond of C≡N…H-Ph with N…H distance of 2.7 Å. The incomplete antiparallel arrangement of the two molecules in each pair remains the molecular polarization, so that the microscopic optical nonlinearity of each PSDCM pair is not entirely offset. The structural difference between PSDCM-(I) and PSDCM–(II) phases are mainly due to the spatial arrangement of PSDCM pairs, which results in the very different macroscopic optical nonlinearity. As shown in Fig. 6, in PSDCM-(I) crystal the acentric PSDCM pairs arrange in parallel and make the optical nonlinearity additive, while in PSDCM-(II) crystal the acentric PSDCM pairs crystallize in a centric space group and counteracts the optical nonlinearity completely.

Interestingly, the two polymorphs for PSDCM, centrosymmetric and acentric, are coincidentally similar to those for 2-(3-(2-(4-pyrrolidinphenyl)-vinyl)-5,5-dimethylcyclohex-2-enylidene)malononitrile (PyT1(I) and Pyt1(II)) obtained in the work of Kwon et al,[22] in which they mainly focused on the selective growth of polyene crystals with different morphologies and polymorphs induced by the tailor-made auxiliaries. It should be emphasized that actually the electron donor groups in PyT1 and PSDCM are very different; in the former molecule the electron donor is pyrrolidinyl group, while in the latter molecule it is phenyl group. The different basic building units result in the different single-crystal growth behaviors and physiochemical properties in the two crystals (see the Supporting Information).

Since the PSDCM-(I) crystal have the potential to be a good NLO material in the IR and THz spectral regions, its thermal and optical properties were measured and OH1 was chosen as the reference sample. Fig. 7 shows the thermal gravimetric analysis (TGA) and differential scanning calorimetry (DSC) thermal diagrams for the PSDCM-(I) crystal. The TGA curve reveals a lower thermal stability with the initial weight-loss temperature (T_i) of 279°C in PSDCM-(I) compared with OH1 (325°C) [10]. The DSC curve of PSDCM-(I) clearly exhibites a sharp endothermic peak at 241°C in the heating curve, which shows a higher melting temperature (T_m) than that in OH1 (212°C) [10]. The temperature difference ΔT of about 38°C between T_m and T_i is smaller than OH1.

The optical absorption curves of PSDCM and OH1 from 300 nm to 1000 nm are displayed in Fig. 8. It clearly demonstrates that the short wavelength cut-offs of the two crystals are located at 575 nm and 589 nm, respectively, corresponding to the energy bandgaps of 2.16 eV and 2.11 eV as obtained by the straightforward extrapolation method. [31]

The powder SHG experiments reveal that PSDCM-(I) exhibits a relatively strong SHG response with about 0.3 times of the OH1 powder for the same particle sizes. At the same time, we performed the first-principles calculations, and Table 3 lists the comparison of the calculated SHG coefficients (and powder SHG effect) between PSDCM-(I) and OH1. One can see that our calculated SHG coefficients for OH1 are in good agreement with the previous measured values (e.g. d_{33}=120±10 pm/V at λ=1.9 μm), [11] confirming the validity of plane-wave pseudopotential method on the NLO calculations in the CLP crystals. The calculated powder SHG effect of PSDCM-(I) is about 0.2 times that of OH1, which is also consistent with the measured result. It should be noted that in this study only the electronic contribution to the SHG effect is considered. In fact, for the NLO crystals used in the low frequency regions (especially in the THz region) the lattice vibrations (or phonons) would greatly affect the optical properties in these regions. However, due to the fact that the energy of the fundamental laser (λ=2.09 μm, or 0.59 eV) is much larger than that of phonons (< tens of THz, or several meV), the contribution of phonons to the optical properties in PSDCM-(I) under the measured condition is neglectably small and can be completely ignored. In addition, since the energy bandgaps of PSDCM-(I) and OH1 (> 2.1 eV) are much larger than that of the fundamental laser, it is expected that the Kleinman symmetry of the d_{ij} tenors is obeyed and the dispersion of SHG effect is small in the two crystals.

To clarify the large deviation between the SHG effects in PSDCM-(I) and OH1, the SHG coefficients of a single molecule in the two crystals were investigated. In the computer simulations the single molecule is put into a very large cubic supercell ($25\times25\times25A^3$, with the molecular polarization axis along the *z*-axis) in order to eliminate the spurious molecular interactions between periodic images. According to the two-level model,[32] the first hyperpolarizability can be roughly estimated by λ_{max}. Namely, the λ_{max} order is in consistent with the relative magnitude of first hyperpolarizability. This conclusion is also verified by our results on PSDCM-(I), OH1 and DAT2: PSDCM-(I) has a quite short absorption wavelength

of 407nm compared with OH1 (425nm) and DAT2 (500nm), and the calculated first hyperpolarizability (~d_{33}) of a PSDCM molecule (1.5 pm/V) is rather smaller than that of OH1 (2.1 pm/V) and DAT2 (9.6 pm/V). It is revealed that the largest SHG coefficient along the polarization axis of a single OH1 molecule (d_{33}=2.1 pm/V) is larger than that of a PSDCM molecule (d_{33}=1.5 pm/V). It is because the stronger electron-donating ability of hydroxyl group in OH1 compared with phenyl group in PSDCM result in the larger second first hyperpolarizability in the former molecule. However, the ratio of the molecular SHG coefficients between OH1 and PSDCM (~1.4) is much less than that of the overall SHG effects in crystals (> 3.3). This implies that the magnitude of SHG effects in the two crystals is dominantly determined by the spatial orientation of molecules rather than the second first hyperpolarizability of individual molecules. Indeed, the nearly anti-parallel molecular arrangement in each molecular pairs (see Fig. 4(a)) seriously cancels out the microscopic second-order susceptibility in PSDCM-(I). In addition, in another CLP crystal 2-(3-(2-(4-dimethylaminophenyl)vinyl)- 5,5-dimethylcyclohex-2- enylidene) malononitrile (DAT2) the dimethylamino [-N(CH_3)$_2$] group has an extremely strong donor characteristics. But this crystal also merely exhibits a powder SHG intensity of about 0.25 times that of OH1 at a fundamental wavelength of 1.9 μm,[10, 16] since it crystallizes in the same monoclinic space-group ($P2_1$) as PSDCM-(I) with the similar non-optimized molecular packing manner. Therefore, one may conclude that besides the hyperpolarizability of the constituent single molecule, the spatial arrangement pattern of the CLP molecules would be also very important for the generation of strong macroscopic NLO effects.

Conclusions

In this work, five new configurationally locked polyene crystals PSDCM-(I), PSDCM-(II), MTDCM, TSDCM, DTCM, DMSCM were synthesized and their crystal structures were determinted by single-crystal X-ray diffraction. Among these organic compounds, the PSDCM-(I) crystal possesses a noncentrosymmetric monoclinic space group $P2_1$ and exhibits a relatively large SHG effect of 0.3 × OH1, consistent with the first-principles results. Combined with the relatively large energy bandgap of 2.16 eV and the comparatively high melting temperature of 241°C, PSDCM-(I) has the potential for NLO applications, e.g., in the IR or even THz spectral region.

Acknowledgements

This work was supported by the National Basic Research Project of China (Grant no. 2010CB630701) and the National Natural Science Foundation of China under grant No 11174297. The authors acknowledge Prof. Jiyong Yao, Technical Institute of Physics and Chemistry, CAS, for crystal structure suggestions.

Notes and references

[a] *Beijing Center for Crystal Research and Development, Key Laboratory of Functional Crystals and Laser Technology, Technical Institute of Physics and Chemistry, Chinese Academy of Sciences, Beijing 100190, China. Email: liyin2109@163.com*

[b] *University of Chinese Academy of Sciences, Beijing 100049, PR China*

† Electronic Supplementary Information (ESI) available: Crystallographic data in CIF format for CCDC 994851, 994852, 994853, 994854, 994855, 1003775, and the difference between PyT1 and PSDCM. See DOI: 10.1039/b000000x/

1 L. Mutter, M. Koechlin, M. Jazbinsek, P. Günter, *Opt. Express*, 2007, **15**, 16828.
2 C. Diederichs, J. Tignon, G. Dasbach, C. Ciuti, A. Lemaitre, J. Bloch,P. Roussignol, C. Delalande, *Nature,* 2006, **440**, 904.
3 B. Ferguson, X. C. Zhang, *Nat. Mater.,* 2002, **1**, 26.
4 S. R. Marder, J. W. Perry, *Science,* 1994, **263**, 1706.
5 C. Bosshard, R.Spreiter, L. Degiorgi, P. Gunter, *Phys. Rev. B: Condens. Matter.,* 2002, **66**, 205107.
6 S. R.Marder,J. W.Perry,C. P. Yakymyshyn, *Chem.Mater.,* 1994, **6**, 1137.
7 U. Meier, M. Bösch, C. Bosshard, P. Günter, *Synthetic Metals,* 2000, **109**,19.
8 L. Mutter, F. D. J. Brunner, Z. Yang, M. Jazbinšek, P. Günter, *J. Opt. Soc. Am. B.,* 2007, **24**, 2556.
9 M. Stillhart, A. Schneider, P. Günter, *J. Opt. Soc. Am. B,* 2008, **25**, 1914.
10 O. P. Kwon, S. J. Kwon, M. Jazbinšek, F. D. J. Brunner, J. I. Seo, C. Hunziker, A. Schneider, H. Yun, Y. S. Lee, P. Günter, *Adv. Funct. Mater.,* 2008, **18**, 3242.
11 C. Hunziker, S. J. Kwon, H. Figi, F. Juvalta, O. P. Kwon, M. Jazbinšek, P. Günter, *J. Opt. Soc. Am. B,* 2008, **25**,1678.
12 F. D.J. Brunner, O. P. Kwon, S. J. Kwon, M. Jazbinšek, A. Schneider, P. Günter, *Optics Express,* **16**, 16496.
13 Y. Li, J. X. Zhang, G. Q. Zhang, L. L. Wu, P. Z. Fu, Y. C. Wu, *Journal of Crystal Growth,* 2011, **327**, 127.
14 P. X. Liu, D. G. Xu, Y. Li, X. Y. Zhang, Y. Y. Wang, J. Q. Yao, Y. C. Wu, *EPL.,* 2014, **106**, 60001
15 Y. Li, Z. A. Wu, X. Y. Zhang, L. Wang, J. X. Zhang, Y. C. Wu, *Journal of Crystal Growth,* 2014, **402**, 53.
16 O. P. Kwon, B. Ruiz, A. Choubey, L. Mutter, A. Schneider, M. Jazbinšek, P. Günter, *Chem. Mater.,* 2006, **18**, 4049.
17 O. P. Kwon, S. J. Kwon, M. Stillhart, M. Jazbinšek, A. Schneider, V. Gramlich, P. Günter, *Crystal Growth & Design,* 2007, **7**, 2517.
18 J. Y. Seo, S. B. Choi, M. Jazbinšek, F. Rotermund, P. Günter, O. P. Kwon, *Crystal Growth & Design,* 2009, **9**, 5003.
19 O. P. Kwon, S. J. Kwon, M. Jazbinšek, J. Y. Seo, J. T. Kim, J. I. Seo, Y. S. Lee, H. Yun, P. Günter, *Chem. Mater.,* 2011, **23**, 239.
20 O. P. Kwon, S. J. Kwon, M. Jazbinšek, A. Choubey, V. Gramlich, P. Günter, *Adv. Funct. Mater.,* 2007, **17**, 1750.
21 S. J. Kwon, O. P. Kwon, M. Jazbinšek, V. Gramlich, P. Günter, *Chem. Commun.,* 2006, 3729.
22 O. P. Kwon, S. J. Kwon, M. Jazbinsek, A. Choubey, P. A. Losio, V. Gramlich, P. Günter, *Crystal Growth & Design,* 2006, **6**, 2327.
23 R. Lemke, *Synthesis,* 1974, 359.
24 S. K. Kurtz, T. T. Perry, *Journal of Applied Physics,* 1968, **39**, 3798.

25 S. J. Clark, M. D. Segall, C. J. Pickard, P. J. Hasnip, M. J. Probert, Refson, K. M. C. Payne, *Zeitschrift Fur Kristallographie,* 2005, **220**, 567.
26 W. Kohn, L. J. Sham, *Physical Review,* 1965, **140**, 1133.
27 (a) J. P. Perdew, A. Zunger, *Physical Review B,* 1981, **23**, 5048; (b) D. M. Ceperley, B. J. Alder, *Physical Review Letters,* 1980, **45**, 566.
28 D. Vanderbilt, *Physical Review B,* 1990, **41**, 7892.
29 H. J. Monkhorst, J. D.Pack, *Physical Review B,* 1976, **13**, 5188.
30 (a) Z. S. Lin, J. Lin, Z. Z. Wang, Y. C. Wu, N. Ye, C. T. Chen, R. K. Li, *Journal of Physics: Condensed Matter,* 2001, **13**, R369; (b) Z. S. Lin, X. X. Jiang, L. Kang, P. F. Gong, S. Y. Luo and M. H. Lee, *J. Phys. D: Appl. Phys.* 2014, **47**, 253001.
31 O. Schevciw, W. B. White, *Mater. Res. Bull.,* 1983, **18**, 1059.
32 J. L. Oudar, D. S. Chemla, *J. Chem. Phys.,* 1977, **66**, 2664.
33 J. Y. Seo, M. Jazbinsek, E. Y. Choi, S. H. Lee, H. Yun, J. T. Kim, Y. S. Lee, O.P. Kwon, *Crystal Growth & Design,* 2013, **13**, 1014.

Highlight

PSDCM-(I) crystal with phenyl as electron donor in molecule structure exhibits a large powder SHG intensity about 0.3 × OH1.

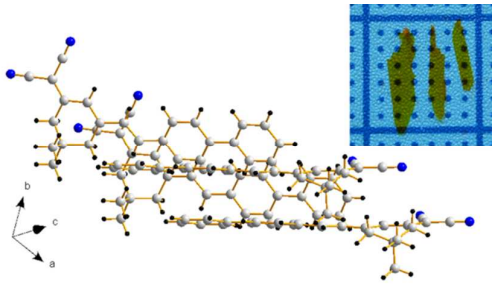

Figure Captions

Fig. 1 The synthetic route of PSDCM as an example.

Fig. 2 The grown PSDCM crystals by (a) cooling method in acetonitrile; (b) slow evaporation from dichloromethane.

Fig. 3 Chemical structures of OH1 and the investigated CLP crystals.

Fig. 4 ORTEP drawing of PSDCM molecule in the (a) phase (I) crystalline state and (b) phase (II) crystalline state.

Fig. 5 Geometrical structure in a PSDCM-(I) crystal (a) view along the *a*-axis and (b) spatial stacking pattern of two PSDCM molecules.

Fig. 6 Top view of the acentric pairs in (a) PSDCM-(I) and (b) PSDCM-(II).

Fig. 7 TGA and DSC thermal diagrams of PSDCM-(I) crystal.

Fig. 8 UV-vis-NIR diffuse reflectance spectra of PSDCM-(I) and OH1 crystals. The short wavelength cut-offs are determined by the straightforward extrapolation method (straight lines).

Figures

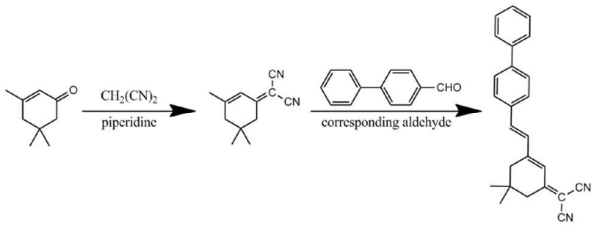

Fig. 1 The synthetic route to PSDCM as an example.

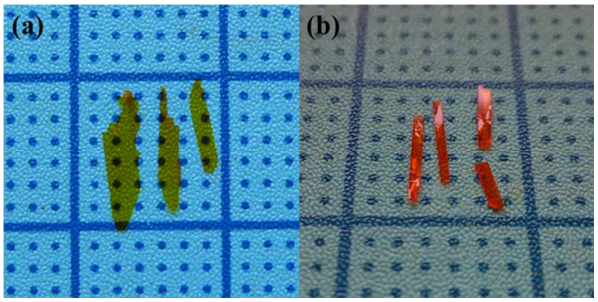

Fig. 2 The grown PSDCM crystals by (a) slow evaporation from dichloromethane; (b) cooling method in acetonitrile.

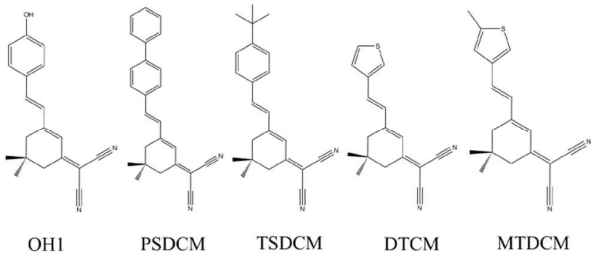

Fig. 3 Chemical structures of OH1 and the investigated CLP crystals.

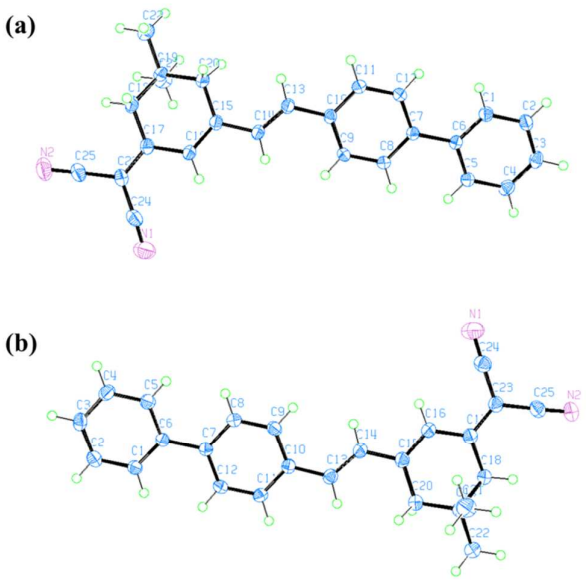

Fig. 4 ORTEP drawing of PSDCM molecule in the (a) phase (I) crystalline state and (b) phase (II) crystalline state.

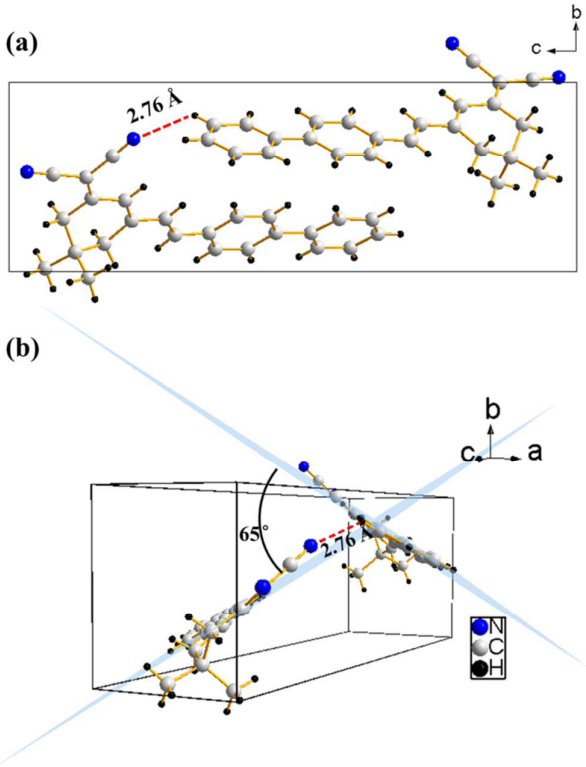

Fig. 5 Geometrical structure in a PSDCM-(I) crystal (a) view along the a-axis and (b) spatial stacking pattern of two PSDCM molecules.

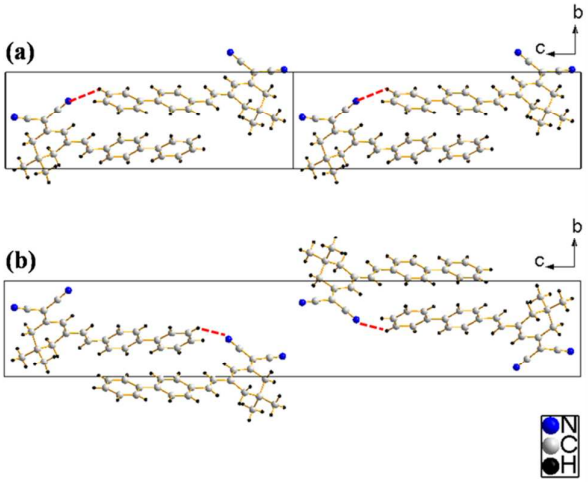

Fig. 6 Top view of the acentric pairs in (a) PSDCM-(I) and (b) PSDCM-(II).

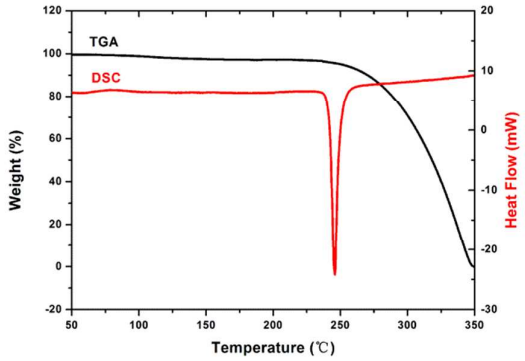

Fig. 7 TGA and DSC thermal diagrams of PSDCM-(I) crystal.

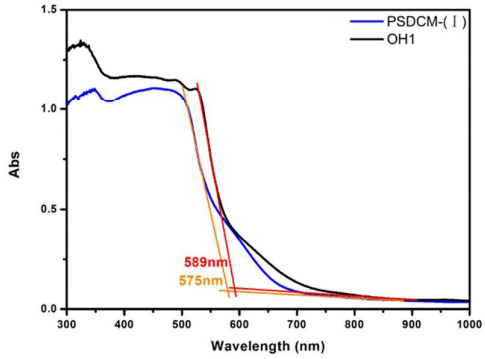

Fig. 8 UV-vis-NIR diffuse reflectance spectra of PSDCM-(I) and OH1 crystals. The short wavelength cut-offs are determined by the straightforward extrapolation method[31] (straight lines).

Tables

Table 1. Crystallographic data and structure refinements for the six CLP crystals[a]

	PSDCM-(I)	PSDCM-(II)	DMSCM	TSDCM	DTCM	MTDCM
formula	$C_{25}H_{22}N_2$	$C_{25}H_{22}N_2$	$C_{20}H_{20}N_2S$	$C_{23}H_{26}N_2$	$C_{17}H_{16}N_2S$	$C_{18}H_{18}N_2S$
f_w	350.45	350.45	320.44	330.46	280.38	294.40
crystal system	monoclinic	monoclinic	monoclinic	triclinic	triclinic	monoclinic
space group	$P2_1$	$P2_1/c$	$P2_1/c$	$P\bar{1}$	$P\bar{1}$	$P2_1/c$
a (Å)	5.9539(12)	5.9789(15)	6.1852(16)	8.7434(13)	8.241(2)	9.1048(19)
b (Å)	7.3758(15)	7.3765(18)	17.016(5)	13.538(2)	9.610(3)	7.4536(15)
c (Å)	22.019(5)	43.952(11)	16.637(4)	17.321(3)	9.790(3)	23.795(5)
α (deg)	90.00	90.00	90.00	88.079(5)	87.334(9)	90.00
β (deg)	91.787(3)	91.422(4)	91.581(4)	84.857(5)	71.536(8)	95.952(4)
γ (deg)	90.00	90.00	90.00	77.108(5)	84.334(9)	90.00
V (Å^3)	966.5(3)	1937.8(8)	1750.3(8)	1990.4(6)	731.8(4)	1606.1(6)
Z	2	4	4	4	2	4
R_1 ($> 2\sigma(I)$)	0.0398	0.0892	0.0419	0.0599	0.0387	0.0495
wR_2(all data)	0.0996	0.2094	0.0937	0.1395	0.0884	0.1218
CCDC No.	994854	1003775	994851	994855	994852	994853

[a] For all structures, T=153(2) K

Table 2. The melting point (T_m) and initial weight-loss temperature (T_i) of the five crystals

	Tm /°C	Ti /°C
PSDCM-(I)	241	279
PSDCM-(II)	239	318
DMSCM	170	238
TSDCM	169	242
DTCM	204	251
MTDCM	161	221

Table 3. Comparison of the calculated SHG coefficients of OH1 and PSDCM-(I) by the first-principles method (unit: pm/V). The powder SHG effect is obtained from the calculated SHG components using Kurtz and Perry's formula[30]

	OH1	PSDCM-(I)
SHG coefficients	d_{31}= 15.0	d_{14}= -5.4
	d_{32}= 12.5	d_{21}= 0.7
	d_{33}= 105.6	d_{23}= -12.1
Powder SHG effect	50.8	8.9 (0.2×OH1)